

PREPARATION OF MESOPOROUS TITANIA-SILICA AEROGELS BY CO₂ SUPERCRITICAL EXTRACTION

Silvester Tursiloadi^{*}, Dinie Mansur, Yeny Meliana and Ruslan Efendi

Research Center for Chemistry, Indonesian Institute of Sciences, Kawasan PUSPIPTEK, Serpong, Tangerang 15314, Indonesia

Received 15 April 2007; Accepted 1 June 2007

ABSTRACT

Stable anatase is attractive because of its notable functions for photocatalysis and photon-electron transfer. TiO₂-nanoparticles dispersed SiO₂ wet gels were prepared by hydrolysis of Ti(OC₄H₉)₄ and Si(OC₂H₅)₄ in a 2-propanol solution with acid catalyst. The solvent in the wet gels was supercritically extracted using CO₂ at 60 °C and 22 Mpa in one-step. Thermal evolution of the microstructure of the extracted gels (aerogels) was evaluated by XRD measurements, TEM and N₂ adsorption measurements. The as-extracted aerogel with a large specific surface area, more than 365 m²g⁻¹, contained anatase nanoparticles, about 5 nm in diameter. The anatase phase was stable after calcinations at temperatures up to 1000 °C, and BET specific surface area, total pore volume and average pore diameter did not change significantly after calcinations at temperature up to 800 °C.

Keywords: Stable anatase, sol-gel, CO₂ supercritical extraction.

INTRODUCTION

Anatase type titania exhibits high photocatalytic activity, and thus has attracted a great deal of attention in the field of photocatalysts for decomposition of environmental pollutants such as organic halides [1] and for antifouling and antibacterial application [2,3]. However, there are significant challenges in obtaining mesoporous titania with full anatase crystalline domains. On the other hand, at standard pressure (1bar) and normal temperatures, rutile is a thermodynamically more stable phase possessing smaller band gap energy (3.0 eV) than the anatase phase (3.2eV), and lower photocatalytic activity [4,5]. Anatase nanocrystals show higher photocatalytic activities than the bulk crystals because the nanocrystals facilitate the diffusion of excited electrons and holes toward the surface before their recombination [6]. In addition, the anatase nanocrystals must be highly dispersed in the host matrix without aggregation to improve the activity. Mesoporous TiO₂-SiO₂ gel, a combination of highly adsorptive silica matrix and highly photo-active titania nanoparticles, will be an interesting material for photocatalytic applications.

The syntheses of ultrafine titania powders has been investigated using various techniques including hydrothermal treatment, oxidation of titanium powder, and vapor decomposition [7-9]. The sol-gel syntheses are widely used for preparation of transition metal oxides with nanoscale microstructures, and provide excellent chemical homogeneity and the possibility of deriving unique metastable phases at low reaction temperatures. The high porosity and the high specific surface area of material prepared by the sol-gel method make them very attractive from catalytic point of view. However, the titania powders prepared by the sol-gel method are usually amorphous, and the crystallization temperature

is relatively high. The crystallization temperature can be reduced with the hydrothermal treatment, and depends on the temperature of hydrothermal treatment [10,11]. The heat treatment is a significant step with respect to device fabrication. Excessive heating causes mesopore collapse, leading to the formation of dense materials, due to excessive crystal growth and sintering, which in turn will decrease device efficiency [12,13]. Additionally, the localized crystal domain limits the photoactivity of the resultant materials [14-16]. Recently, the preparation of mesoporous titania which has highly porous and a fully crystalline phase domain has been scarcely explored [17,18]. Supercritical extraction techniques are recently used in material science to fabricate highly porous materials [19]. The supercritical extraction technique seems to be a good alternative to overcome the problems of low porosity and low specific surface area of sol-gel derived titania.

In this work, a new route to prepare mesoporous titania with highly porous and full anatase domains of TiO₂-nanoparticles dispersed SiO₂ aerogels were prepared by the sol-gel method and supercritical extraction, and the stability of anatase phase and the porous structure, *i.e.* pore size and specific surface area, has been discussed.

EXPERIMENTAL SECTION

TiO₂-SiO₂ wet gels were prepared by hydrolysis of titanium tetra-n-butoxide Ti(OC₄H₉)₄ (TNB) and tetraethylortosilicate Si(OC₂H₅)₄ (TEOS) in a 2-propanol solution with acid catalyst. The molar ratios used for the synthesis were [TNB+TEOS]: [H₂O]: solvent = 1: 13.4: 127 and [HNO₃]: [TNB+TEOS] = 0.06: 1. The ratios of [TiO₂]: [SiO₂] were 1: 0, 1: 2 and

* Corresponding author. Email: tursilo@gmail.com

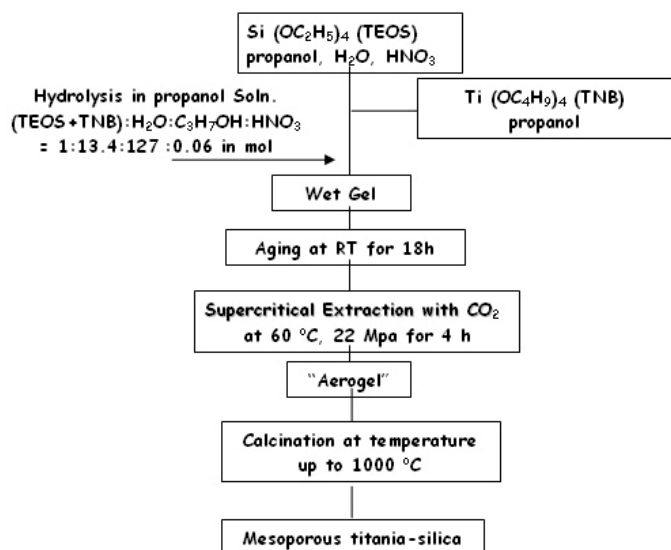


Fig 1. Flowchart of sample preparation

1:4 in mol. The TEOS was firstly dissolved in 2-propanol at room temperature, and a mixture of the catalyst solution, remaining 2-propanol, H₂O and HNO₃ was added, and then stirred for 30 min. After that, TNB was added and then the catalyst solution was added under continuous stirring. The solution gelled around 3h after the addition of the catalyst solution. The gel time was defined as the time required after mixing for the vortex created by the stirring to disappear completely. The wet gel was placed in the flow of supercritical carbon dioxide in a supercritical extraction system at 60 °C and 22 Mpa for 4h. The supercritically extracted aerogels were calcined at 500, 600, 700, 800, 900 and 1000 °C for 2 h in air (Fig 1).

Changes in the microstructure of the aerogels during heating were evaluated by measurements of N₂ adsorption (Quantachrome, Autosorb). The specific surface area and pore volume of aerogels, before and after calcinations, were estimated by the BET and Barret-Joyner-Halenda (BJH) method [20] using N₂ desorption curves. The pore and grain sizes of the samples were estimated from the images observed by a transmission electron microscope (TEM, Philips, TECNAI F20). Crystallization behaviors of the samples were detected by an X-ray diffractometer (Rigaku, RAD-C) after calcinations.

RESULT

TG and DTA profiles of TiO₂ and TiO₂-2SiO₂ aerogels are showed in Fig 2 and Fig 3. For the TiO₂ aerogel, weight loss around 5 % was mainly observed at around 80 °C (Fig 2). Beyond 400 °C the sample of TiO₂ aerogel practically lose no more weight. In the DTA curve, the TiO₂ aerogel showed endothermic peak

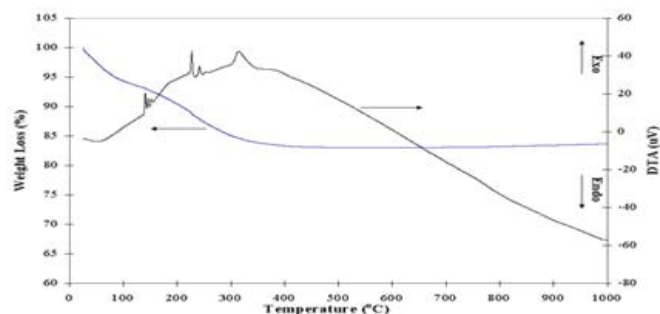


Fig 2. TG-DTA profiles of TiO₂ Aerogel

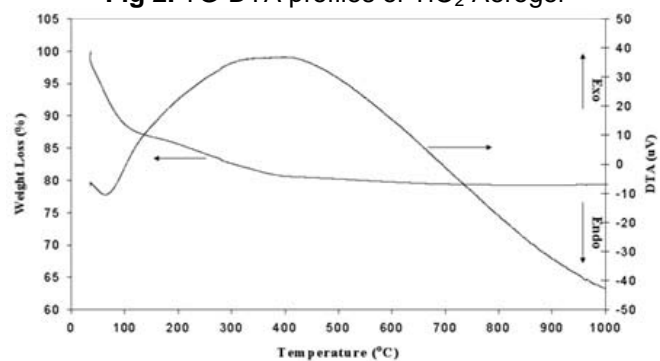


Fig 3. TG-DTA profiles Aerogel of TiO₂-SiO₂

around 80 °C and weak triplet exothermic peaks around 150 and 250 °C which accompanied weight loss around 8% and 5% respectively. The broad exothermic peak at around 310 °C is followed by weight loss around 4% also observed. For the TiO₂-2SiO₂ aerogel (Fig 3), weight loss around 13 % was mainly observed at around 100 °C.

Beyond 400 °C, the sample of TiO₂-2SiO₂ aerogel loses practically no more weight. In the DTA curve, the TiO₂-2SiO₂ aerogel showed endothermic peak around 100 °C accompanied weight loss around 13% and around 400 °C weight loss around 5% and no exothermic peak. Endothermic peaks appeared in almost the same temperature region for both samples namely at around 100 °C as the evaporation of water and 2-propanol as hydrolyzing reagent and solvent, respectively.

The X-ray powder diffraction peaks of anatase were found for the as-extracted TiO₂ aerogel (Fig 4). The anatase phase was stable after calcination at 500 °C. After calcination at 600 °C, weak peaks of rutile were found along with the anatase peaks. After calcination at 700 °C, the diffraction peaks of anatase disappeared and only the peaks of rutile were found. The X-ray diffraction peaks of anatase were found for the as-prepared TiO₂-2SiO₂ aerogel, too (Fig 5). The anatase phase in the TiO₂-2SiO₂ aerogel was stable after calcinations at temperatures up to 1000 °C, and no peaks of rutile were observed (Fig 5). The as-extracted gel of TiO₂-4SiO₂ was amorphous by XRD (Fig 6). After calcination at 600 °C, very weak peaks of

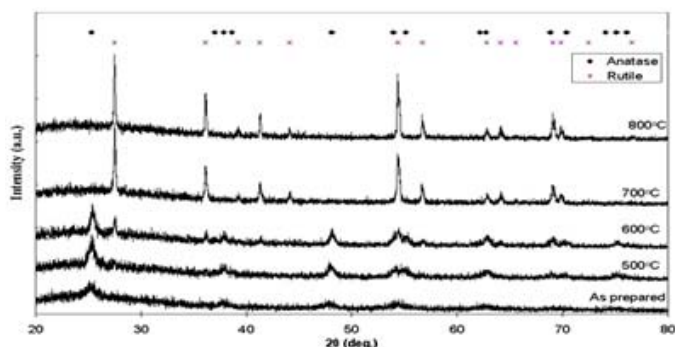


Fig 4. XRD patterns of the TiO₂ aerogels as-prepared and after calcination at various temperatures

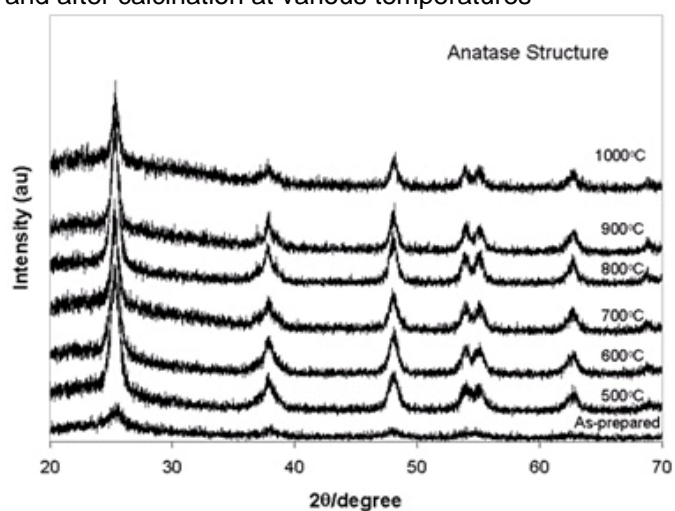


Fig 5. XRD patterns of the TiO₂-2SiO₂ aerogels as-prepared and after calcination at various temperatures

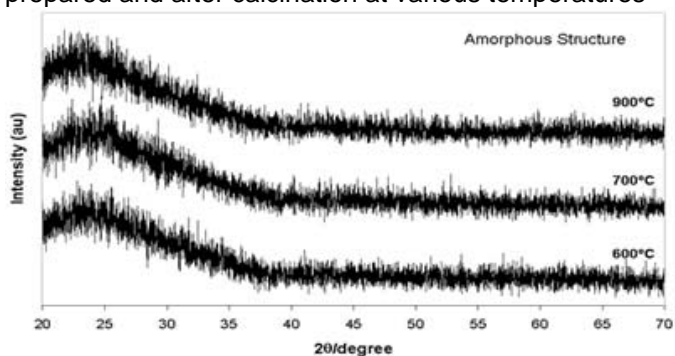


Fig 6. XRD patterns of the TiO₂-4SiO₂ aerogels after calcination at various temperatures

anatase can be found, and hardly changed by calcinations at higher temperatures up to 900°C (Fig 6).

Fig 7 shows the TEM images and electron diffraction patterns for the as-prepared aerogels of TiO₂ and TiO₂-SiO₂. The crystalline structures were assigned to anatase from the electron diffraction patterns for TiO₂ and TiO₂-2SiO₂ aerogels. Many small anatase particles were observed throughout the as-prepared TiO₂ and

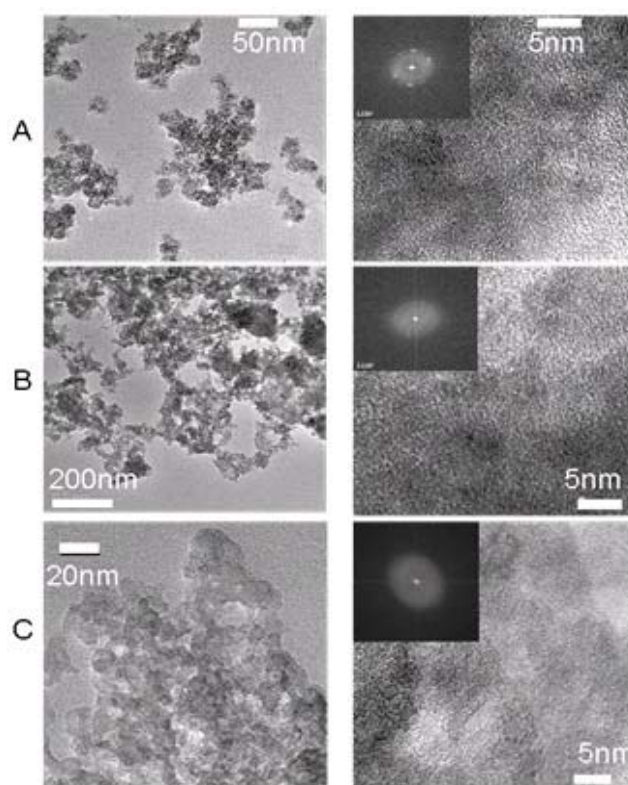


Fig 7. TEM images and electron diffraction patterns for the as-extracted aerogels; (a) TiO₂, (b) TiO₂-2SiO₂ and (c) TiO₂-4SiO₂

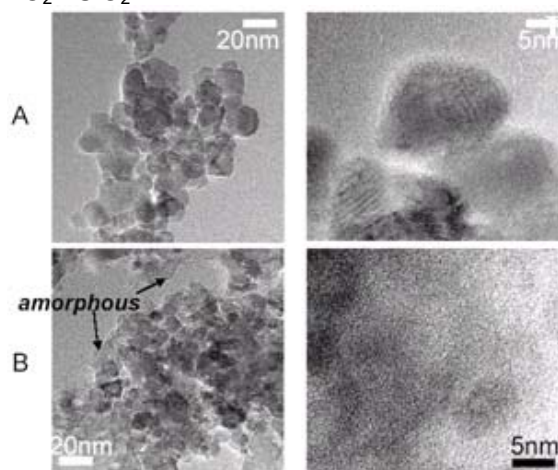


Fig 8. TEM images for the aerogels after calcination at 500°C; (a) TiO₂ and (b) TiO₂-2SiO₂

TiO₂-2SiO₂ aerogels (Fig 7 (a) and (b)). The particle size of anatase in the as-prepared TiO₂- and the TiO₂-2SiO₂ aerogels was about 5 nm in diameter. The TEM images and electron diffraction pattern (Fig. 8(a)) show that the anatase particle size in the TiO₂ aerogel increased about to 13 nm after calcination at 500 °C, and the anatase particle size in the TiO₂-2SiO₂ aerogel increased about to 10 nm (Fig 8(b)). Amorphous particles were found in addition to the anatase particles

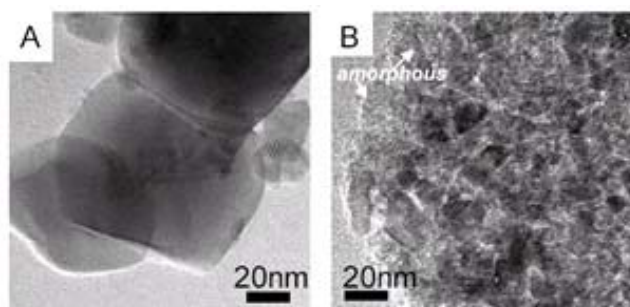


Fig 9. TEM images for the aerogels after calcination at 700°C; (a) TiO₂ and (b) TiO₂-2SiO₂

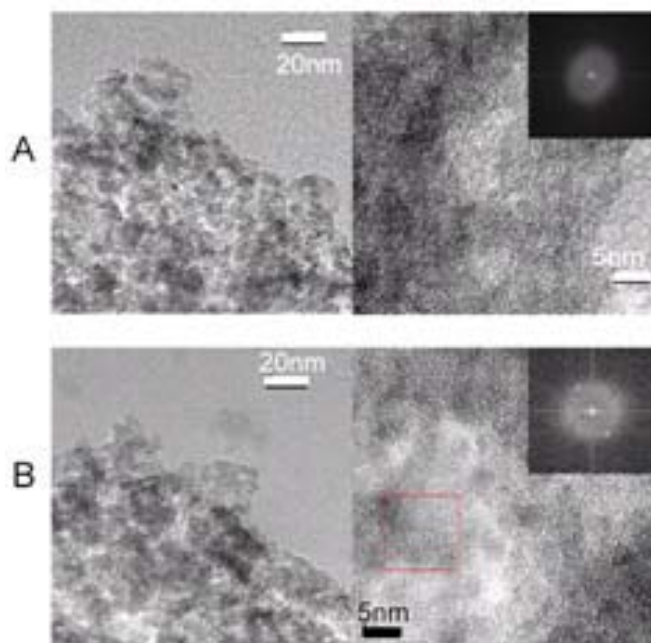


Fig 10. TEM images and electron diffraction patterns for TiO₂-4SiO₂ calcined (a) at 700°C and (b) at 800°C

for the TiO₂-2SiO₂ aerogel, but not for the TiO₂ aerogel. After calcination at 700 °C, the particle size of the TiO₂ aerogel increased significantly, about 90 nm in diameter, but the anatase particle size of the TiO₂-2SiO₂ aerogel did not change significantly i.e. 10 nm (Figs. 9(a) and (b)). Amorphous particles were still found for the TiO₂-2SiO₂ aerogel in addition to the anatase particles.

Crystalline nanoparticles were hardly found for the TiO₂-4SiO₂ aerogels after calcinations at temperatures up to 700 °C. However, anatase nanoparticles, about 5 nm in diameter, were found for the TiO₂-4SiO₂ aerogel after calcination at 800 °C (Fig 10(b)).

Table 1 shows the effect of calcination temperatures on the total pore volume, the specific surface area and the average pore diameter of the aerogels. The total pore volume of the as-prepared TiO₂ was 0.56 cm³g⁻¹, and after calcinations at 600 °C, it became 0.35 cm³g⁻¹ and was larger than the total pore volume of the TiO₂-2SiO₂ aerogel, 0.25 and 0.28 cm³g⁻¹, respectively. After calcinations at temperatures higher

Table 1. Specific surface area, cumulative pore volume, and average pore diameter of the TiO₂ and TiO₂-SiO₂ aerogels after calcination at various temperatures.^a

	as-extracted	500 °C	600 °C	700 °C	800 °C
TiO₂					
Surface area (m ² g ⁻¹)	195	90	58	19	5
Pore volume (cm ³ g ⁻¹)	0.555	0.487	0.345	0.164	0.053
Average pore diameter (nm)	12.8	18.7	20.1	36.5	51.6
TiO₂-SiO₂ 1:2					
Surface area (m ² g ⁻¹)	365	338	309	296	260
Pore volume (cm ³ g ⁻¹)	0.249	0.299	0.282	0.274	0.253
Average pore diameter (nm)	3.2	3.8	3.9	3.9	4.2
TiO₂-SiO₂ 1:4					
Surface area (m ² g ⁻¹)	566	435	392	329	273
Pore volume (cm ³ g ⁻¹)	1.136	0.808	0.836	0.736	0.746
Average pore diameter (nm)	8.1	7.6	8.7	9.2	11.4

^a The accuracy of N₂ adsorption measurements was 0.1 %, and the reproducibility of these values for each sample was within 10 %.

than 600 °C, the total pore volume of the TiO₂ aerogel decreased remarkably and became smaller than that of the TiO₂-2SiO₂ aerogel. However, the pore volume for the TiO₂-2SiO₂ aerogels after calcinations at temperatures up to 800 °C hardly changed. The specific surface area of the as-extracted TiO₂ aerogel, 195 m²g⁻¹, was smaller than that of the as-extracted TiO₂-2SiO₂ aerogel, 365 m²g⁻¹, and it drastically decreased after calcination at 500 °C, 90 m²g⁻¹. On the contrary, changes in the specific surface area of the TiO₂-2SiO₂ aerogel by calcinations were not significant. After calcinations at 800 °C, the specific surface area of the TiO₂-2SiO₂ aerogel was still large, 260 m²g⁻¹. Also, the changes in the average pore diameter of the TiO₂-2SiO₂ aerogel by calcinations, from 3.2 nm as-extracted to 4.2 nm after calcinations at 800 °C, were not significant in comparison with the changes of the TiO₂ aerogel, from 12.8 nm as-extracted to 51.6 nm after calcinations at 800 °C. These results show that the porous structure of the TiO₂-2SiO₂ aerogel was thermally stable at temperatures up to 800 °C in comparison with the TiO₂ aerogel. The as-extracted TiO₂-4SiO₂ aerogels had larger specific surface area, pore volume and pore size than other aerogels, and they were still large after calcination at 800 °C.

DISCUSSION

Exothermic peaks are hardly found for the $\text{TiO}_2\text{-2SiO}_2$ aerogel. It may be caused by the solvent (alcohol) that hardly remained in the $\text{TiO}_2\text{-2SiO}_2$ aerogel. The solvent of the $\text{TiO}_2\text{-2SiO}_2$ may be removed by the supercritical extraction. The temperature needed to eliminate residual alkoxy group of TiO_2 aerogel were found up to 400°C that is indicated that a lot of residual alkoxy group still remain.

By the supercritical CO_2 -extraction in one-step, highly porous $\text{TiO}_2\text{-SiO}_2$ gels with a large specific surface area have been obtained. Aerogels are usually prepared by the two-step drying process, *i.e.* substitution of solvent in wet gels with liquid CO_2 and then supercritical extraction. The substitution of solvent usually needs a long time and complex operations, and therefore, the one-step extraction method will be the better alternative. The effect of CO_2 supercritical extraction on the crystallization can be seen in Fig 4 and Fig 5. Under the high pressure during the CO_2 supercritical extraction (22 Mpa), crystalline anatase nanoparticles were formed for both of the TiO_2 and the $\text{TiO}_2\text{-2SiO}_2$ aerogel. The as-prepared $\text{TiO}_2\text{-4SiO}_2$ aerogel is amorphous by XRD (Fig 6), probably due to the low concentration of crystalline phase. After calcinations at 800°C , the electron diffraction pattern for small particles in the $\text{TiO}_2\text{-4SiO}_2$ aerogel shows the anatase structure. Anatase phase cannot be found if drying is performed under an ambient pressure. In general, the structure of anatase is formed at temperatures higher than 400°C [10,21]. However, it was reported previously that anatase phase can be found for TiO_2 gel film after hydrothermal treatment at temperatures in the range between 80°C and 180°C [21]. Water vapor was considered to enhance the crystallization of TiO_2 gel through cleavage of Ti-O-Ti bond by hydrolysis [21]. Under high pressure during the supercritical extraction, residual H_2O may enhance the deposition of anatase. On the other hand, solubility of substances into supercritical fluids is usually high, and it can be considered that anatase nanoparticles are formed in supercritical CO_2 by the solution-deposition mechanism from amorphous TiO_2 . However, the solubility of TiO_2 in supercritical CO_2 is not known, and the further discussion should be needed.

The relationship with anatase nucleation and role of SiO_2 were show in Fig 11(a) and (b). The anatase nanoparticles in the TiO_2 aerogel, about 5nm in diameter (Fig 7(a)), grow up to ca. 13 nm after calcinations at 500°C (Fig 8(a)), the diffraction peaks of rutile are found at 600°C (Fig 4), and the particles of rutile grow up to ca. 90 nm after calcinations at 700°C (Fig 9(a), Fig 11(a)). On the contrary, grain growth of anatase nanoparticles in the $\text{TiO}_2\text{-2SiO}_2$ aerogels was hardly observed at temperatures up to 700°C (Fig 8(b) and Fig 9(b)). The

grain growth is restricted with addition of SiO_2 (Fig 11(b)). Anatase nanoparticles in the $\text{TiO}_2\text{-2SiO}_2$ aerogel are surrounded with SiO_2 nanoparticles and highly dispersed, thus the grain growth rate is low (Fig 11(b)). Also, a large amount of SiO_2 will retard the crystallization of TiO_2 and the phase transition from anatase to rutile, probably due to the small particle size of anatase (Fig 14(b)). After calcinations at 600°C , diffraction peaks of rutile were found for the TiO_2 aerogel, but not for the $\text{TiO}_2\text{-2SiO}_2$ aerogels. The shift of crystallization- and phase transition temperatures of small particles and thin films from those of bulk materials, usually higher temperatures, is often reported.

Crystallization or phase transformations take place through nucleation and growth processes. The Gibb's free energy is difference between the amorphous and crystalline phases or between two crystalline phases [22,23]. In the phase transformation of nanocrystalline anatase particles of TiO_2 shows in Fig 11(a). Interface nucleation step **A**, nucleation of rutile starts within the interface between two contacting anatase particles, and the nucleation rate is determined by the probability of contact of two anatase particles [24]. Nuclei growth step **B**, as for any nucleation event, the formation of a stable nucleus is dependent upon interfacial energy. Fluctuation of a rutile nucleus within an anatase particle of around critical size for rutile would almost certainly result in rapid transformation of the entire particle (Fig. 11(a)), removing the interfacial energy contribution. The particle size in diameter of anatase phase of TiO_2 did not change after calcination up to 600°C , namely 13 nm (step **A** and **B**). Thus, the critical nucleus size of TiO_2 is 13 nm (Table 1 and Fig 8(a)). Formation of a rutile particle steps **C**, involves growth at the particle-particle neck from constituents evidently provided by surface diffusion. The growth of rutile may happen when a rutile crystallite comes into contact with an anatase crystallite forming a larger rutile crystallite or when two rutile nuclei merge together.

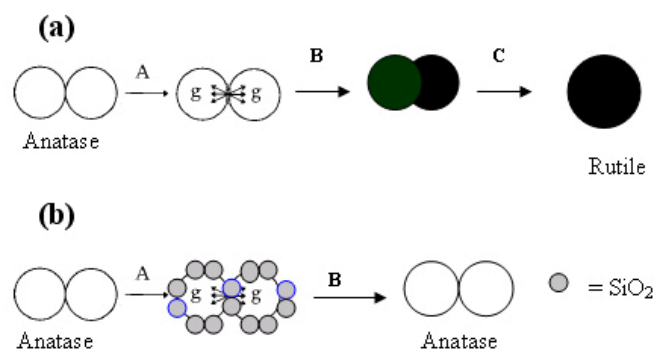


Figure 11. Diagram showing steps involved in the phase transformation of nanocrystalline anatase particles TiO_2 (a) and $\text{TiO}_2\text{-2SiO}_2$ (b). The *g* is the nuclei growth rate.

In the phase transformation of nanocrystalline anatase particles of $\text{TiO}_2\text{-2SiO}_2$ shows in Fig 11(b). Interface nucleation step **A**, nucleation of rutile starts within the interface between two contacting anatase particles, and the nucleation rate is determined by the probability of contact of two anatase particles. Nuclei growth step **B**, is restricted with addition of SiO_2 and critical size for rutile did not achieve. Anatase nanoparticles in the $\text{TiO}_2\text{-2SiO}_2$ aerogel are surrounded with SiO_2 nanoparticles and highly dispersed, thus the nuclei growth rate is low. Also, a large amount of SiO_2 will retard the nuclei growth of TiO_2 and the phase transition from anatase to rutile, probably due to the small particle size of anatase i.e. 10 nm (Fig 9).

The above calcination experiments $\text{TiO}_2\text{-2SiO}_2$ indicate that no anatase transform to rutile. Author consider this to be a consequence of the dependence of thermodynamic stability on particle size, noting that $\text{TiO}_2\text{-2SiO}_2$ and TiO_2 growth rates differ, causing changes in relative stability during thermal treatments. Fig 8 and 9 illustrate the nanocrystalline anatase particles (nm) after calcination at 500 and 700 °C. It is seen that, at particle size of anatase c.a. 13 nm and c.a.10 nm for TiO_2 and $\text{TiO}_2\text{-2SiO}_2$ respectively, anatase is the most stable phase; for particles sizes greater than 13 nm for TiO_2 , rutile is the most stable phase. For $\text{TiO}_2\text{-2SiO}_2$, the particle size is stable in small size namely c.a.10 nm after calcination at 700 °C or more, anatase is the most stable. The thermodynamic of the size effect on the thermal stability of TiO_2 anatase nanoparticles synthesized by MOCVD was reported by Li *et al.*[25]. 12nm anatase had the lowest transformation starting temperature and thermal stability as compared with 17 and 23 nm samples [25]. Anatase is most thermodynamically stable at sizes less than 11nm, brookite is most stable at sizes between 11 and 35 nm, and rutile is most stable at size greater than 35 nm [26].

The specific surface areas of the aerogels after calcinations at various temperatures are shown in Table 1. With increasing calcination temperatures, the specific surface areas of the TiO_2 aerogel decrease drastically, but did not change significantly for $\text{TiO}_2\text{-SiO}_2$ aerogels. This is due to the restriction of the grain growth with addition of SiO_2 .

CONCLUSION

The technique of CO_2 supercritical extraction makes it possible to produce highly porous anatase with small particle size. With addition of a large amount of SiO_2 , the grain growth rate of crystalline TiO_2 , anatase, is restricted, and anatase phase is thermally stabilized. The rutile phase was not found after calcinations at temperatures up to 1000 °C. The transformation sequence among the anatase and rutile is size dependent, because the energies of the anatase and rutile are sufficiently close that they can be reversed by

small differences in surface energy. If particle sizes of the $\text{TiO}_2\text{-2SiO}_2$ and TiO_2 phases are equal or smaller than 13nm anatase is most thermodynamically stable. The rutile is most stable at sizes greater than 13 nm. The specific surface area, the pore volume and the average pore size of $\text{TiO}_2\text{-SiO}_2$ aerogels do not change significantly after calcinations at temperatures up to 800 °C.

REFERENCES

- Weaver, S. and Mills, G., 1997, *J. Phys. Chem. B*, 101, 3769
- Matsubara, H., Tanaka, M., Koyama, S., Hashimoto, K., and Fujishima, A., 1995, *Chem. Lett.*, 1995, 767.
- Ohko, Y., Tryk, D.A., Hashimoto, K., and Fujishima, A., 1998, *J Phys. Chem. B*, 102, 2699
- Sclafani, A., and Herrman, J.M., 1996, *J. Mater. Res.*, 100, 13655
- Kormann, C., Bahnemann D.W., and Hoffmann, M.R., 1988, *J. Phys. Chem.*, 92, 5196
- M. Anpo, T. Shima, S. Kodama, and Y. Kubokawa., 1987, *J. Phys. Chem.*, 91, 4305
- Wang, C., Deng, Z.X., Zhang, G., Fan, S., and Li, Y., 2002, *Powder Technol.*, 125, 39
- Cornell, R.M., Posner A.M., and Quirk, J.P., 1975, *J. Colloid Interface Sci.*, 53, 6
- Mazdiyasi, K.S., Lynch C.T., and Smith, J.S., 1965, *J. Am. Ceram. Soc.*, 48, 372
- Wang, C.C., and Ying, J.Y., 1999, *Chem. Mater.*, 11, 3113
- Ovenstone, J., and Yanagizawa, K., 1999, *Chem. Mater.*, 11, 2770
- Wang, T.Y.Q., Yin, L.X., Palchik, O., Hacoheh, Y.R., Kolytyn, Y., and Gedanken, A., 2001, *Langmuir*, 17, 4131.
- Mason (Ed.). 1990, *Sonochemistry: The Uses of Ultrasound in Chemistry*, Royal Society of Chemistry, Cambridge.
- Fujishima, A., and Honda, K., 1972, *Nature* 238, 37
- Phillips, R., 1983, *Sources and Applications of Ultraviolet Radiation*, p. 124, Academic Press, New York.
- Gedanken, A., Tang, X., Wang, Y., Perkas, N., Kolytyn, Y., Landau, M.V., Vradman, L., and Herskowitz. M., 2001, *Chem. Eur. J.*, 7, 4546.
- Srivastava, D.N., Perkas, N., Gedanken, A., and Felner. I., 2002, *J. Phys. Chem. B* 106, 1878.
- Srivastava, D.N., Chappel, S., Palchik, O., Zaban, A., and Gedanken, A., 2002, *Langmuir* 18, 4160.
- Suh, D.J., Park, T.J., Kim, J.H., and Kim, K.L., 1997, *Chem. Mater.*, 9, 9, 1903
- Barret, E.P., Joyner L.G., and Halenda, P.H., 1951, *J Am. Chem. Soc.*, 73, 373

21. Imai, H., Morimoto, H., Tominaga, A., and Hirashima, H., 1997, *J. Sol-gel Sci. and Tech.*, 10, 45
22. Kasuga, T., Hiramatsu, M., Hoson, A., Sekino, T., and Niihara, K., 1999, *Adv. Mater.* 11, 1307.
23. Kumar, K-N.P., Keizer, K., Burggraaf, A.J., Okubo, T. and Nagamoto, H., 1993, *J. Mater. Chem.* 3, 1151.
24. Zhang, H. and Banfield, D.F., 1999, *Am. Mineralogist*, 84, 528
25. Li, W., Ni, C., Lin, H., Huang, C.P. and Ismat S., 2004, *J. Applied Physics*, 96, 11, 663.
26. Zhang, H. and Banfield, J. F., 2000, *J. Phys. Chem. B*, 104, 3481.